

Correlated electron transport through parallel double-quantum-dot

Rong Lü¹, Zhi-Rong Liu², and Guang-Ming Zhang^{2,1}

¹*Center for Advanced Study, Tsinghua University, Beijing 100084, China;*

²*Department of Physics, Tsinghua University, Beijing 100084, China*

(Dated: June 25, 2018)

We investigate the spectral and transport properties of parallel double-quantum-dot (DQD) system with interdot tunneling coupling in both the equilibrium and nonequilibrium cases. The special geometry of DQD system is considered, in which each dot is connected to two leads by the tunneling barriers. With the help of Keldysh nonequilibrium Green function technique and the equation-of-motion approach, the spectral function and the conductance spectra of DQD system are calculated in two cases with and without the intradot Coulomb interaction, respectively. The exact calculation is performed in the absence of intradot Coulomb interaction. For the case with intradot Coulomb interaction, the Hartree-Fock approximation is applied to truncate the equation of motion for the high-order Green functions at high temperatures. The phenomenon of correlated electron transport is clearly shown in the linear conductance of each dot in the presence of interdot tunneling when setting one dot level and tuning another. The interplay between the intradot Coulomb interaction and the interdot tunneling coupling is displayed.

PACS numbers: 73.63.Kv, 73.23.Hk, 73.21.La

I. INTRODUCTION

Recently, due to the rapid progress in nanotechnologies, quantum transport through DQD system has been the subject of active theoretical and experimental research.¹ Compared to the single quantum dot, the interdot coupling and the intradot on-site Coulomb interaction in DQD system could generate novel many-body states, e. g. the molecular Kondo state.² Apart from its importance in understanding some basic problems in condensed matter physics, the DQD devices are also crucial ingredients in the emerging field of spintronics and several quantum computation schemes designed with the electron spins or with the coherent mode in an artificial molecule.^{3,4}

Transport through DQD system in the Coulomb blockade and the Kondo regimes has already received some theoretical attention, in which two dots are arranged in series,^{5,6,7,8,9,10,11,12,13,14,15,16} parallel^{16,17,18} or T-shape.^{19,20,21} In most of these geometries, the conductance spectra have been studied for electron transport through the whole DQD system, while the electron transport through each individual dot could not be detected. In this paper we consider a new configuration of DQD system (see Fig. 1), in which each quantum dot is connected to two leads by the tunneling barriers. In this geometry, the collected electron transport phenomenon can be investigated by measuring the transport properties through one individual dot when tuning the level of another dot and its interdot coupling. The similar configuration of DQD system has been proposed in Ref. 22, however, the detailed investigation on the spectral and conductance spectra, and the interplay between interdot tunneling coupling and intradot on-site Coulomb interaction has been not discussed yet.

In this paper, by using the Keldysh nonequilibrium Green function technique and equation-of-motion

method, we calculate the spectral and the conductance spectra of tunneling-coupled DQD with and without intradot Coulomb interaction, respectively, in both the equilibrium limit and in the nonequilibrium case. In Sec. II, we formulate the model Hamiltonian of the special geometry of DQD system, and deduce the current formula through each quantum dot.

In Sec. III, for DQD without the intradot Coulomb interaction, we exactly calculate the Green functions, from which both the spectral function and the conductance are obtained, showing the resonant peaks corresponding to the molecular resonant-tunneling bonding and antibonding states. The image of total differential conductance shows "anticrossing" phenomenon when the levels of two dots match. It is interesting to find that in the presence of interdot tunneling coupling, the electron transport through one dot is strongly influenced by the electron transport through another dot, namely, when setting dot 1 level (ϵ_1) and tuning dot 2 level (ϵ_2) the linear conductance of dot 1 (G_{dot1}) shows a dip at the same position of ϵ_2 , where the linear conductance of dot 2 (G_{dot2}) displays a resonant peak. Increasing the interdot tunneling coupling gives rise to a more complicate structure of linear conductances through each dot.

In Sec. IV, we apply the Hartree-Fock approximation to DQD with the intradot Coulomb interaction to truncate the equation of motion for the high-order Green functions, which is known to capture the correct qualitative feature of physics of single quantum dot in the Coulomb blockade regime. Under the same approximation, we also obtain the Keldysh less Green function, which is needed in the self-consistent evaluation of the dot occupation numbers when a finite bias voltage is applied across the system. As the intradot Coulomb interaction becomes the largest energy scale in the single-electron tunneling regime of quantum dot, the intradot Coulomb interaction leads to two groups of peaks in

both the spectral and conductance spectra, and the interdot tunneling coupling causes the splitting of peaks in each group. Compared to the case without the intradot Coulomb interaction, when setting ϵ_1 and tuning ϵ_2 , one more dip in G_{dot1} and resonant peak in G_{dot2} will appear corresponding to the Coulomb interaction energy, which also provides the clear evidence of the correlated electron transport through DQD system. The paper is closed with a brief summary in Sec. V.

II. PHYSICAL MODEL AND CURRENT FORMULA

Quantum dots behave as artificial atoms and single-electron transistors in their charge and energy quantizations due to the small dimensions (compared to the Fermi wavelength). They are often described by the single-impurity Anderson model, in which there is a Coulomb repulsion between electrons in the dot. The parallel DQD system could be modelled by using a two-impurity Anderson model with an extra interdot tunneling corresponding to the electrons hopping between two dots. Each QD is attached to two electronic leads with different chemical potentials by quantum-tunneling barriers. Geometry of the system is shown schematically in Fig. 1. The model Hamiltonian is then given by

$$H = H_{leads} + H_{DD} + H_T. \quad (1)$$

The first term H_{leads} describes the noninteracting electrons in the η -th lead with the electron creation $c_{\mathbf{k}\eta\sigma}^\dagger$ and annihilation $c_{\mathbf{k}\eta\sigma}$ operators,

$$H_{leads} = \sum_{\mathbf{k}, \eta, \sigma} \epsilon_{\mathbf{k}\eta} c_{\mathbf{k}\eta\sigma}^\dagger c_{\mathbf{k}\eta\sigma}, \quad (2)$$

where $\eta = 1, 2, 3, 4$ corresponding to the four leads shown in Fig. 1, \mathbf{k} denotes the wave vector, and σ is the spin index. The second term H_{DD} in Eq. (1) describes the electrons in the dots 1 and 2 with the interdot tunneling coupling t and the intradot on-site Coulomb interaction U ,

$$\begin{aligned} H_{DD} = & \sum_{\sigma} \epsilon_1 d_{1\sigma}^\dagger d_{1\sigma} + \frac{U}{2} \sum_{\sigma} n_{1\sigma} n_{1\bar{\sigma}} \\ & + \sum_{\sigma} \epsilon_2 d_{2\sigma}^\dagger d_{2\sigma} + \frac{U}{2} \sum_{\sigma} n_{2\sigma} n_{2\bar{\sigma}} \\ & - t \sum_{\sigma} (d_{1\sigma}^\dagger d_{2\sigma} + d_{2\sigma}^\dagger d_{1\sigma}). \end{aligned} \quad (3)$$

The last term in Eq. (1) describes the tunneling coupling between dots and the external leads with the tunneling matrix elements V_η ,

$$\begin{aligned} H_T = & \sum_{\mathbf{k}, \sigma} (V_1 c_{\mathbf{k}1\sigma}^\dagger d_{1\sigma} + V_2 c_{\mathbf{k}2\sigma}^\dagger d_{1\sigma} + h.c.) \\ & + \sum_{\mathbf{k}, \sigma} (V_3 c_{\mathbf{k}3\sigma}^\dagger d_{2\sigma} + V_4 c_{\mathbf{k}4\sigma}^\dagger d_{2\sigma} + h.c.). \end{aligned} \quad (4)$$

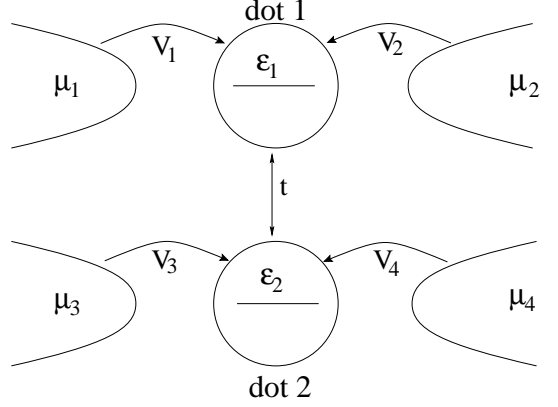


FIG. 1: Schematic diagram of the parallel DQD system studied in this paper.

When we use the Keldysh nonequilibrium Green function technique to express the current through dots 1 and 2, the respective conductance can be written in terms of the distribution functions of leads and the local properties of DQD system. To this end we write the current from the lead 1 to dot 1 as

$$J_1 = -e \langle dN_1/dt \rangle = - (ie/\hbar) \langle [H, N_1] \rangle, \quad (5)$$

where $N_1 = \sum_{\mathbf{k}, \sigma} c_{\mathbf{k}1\sigma}^\dagger c_{\mathbf{k}1\sigma}$. With the help of Eq. (1), one can easily obtain the current from the lead 1 to dot 1 as

$$\begin{aligned} J_1 = & \frac{ie}{\hbar} \sum_{\mathbf{k}, \sigma} (V_1 \langle c_{\mathbf{k}1\sigma}^\dagger d_{1\sigma} \rangle - V_1^* \langle d_{1\sigma}^\dagger c_{\mathbf{k}1\sigma} \rangle) \\ = & \frac{e}{\hbar} \sum_{\mathbf{k}, \sigma} \int \frac{d\omega}{2\pi} [V_1 G_{1\sigma, \mathbf{k}1\sigma}^<(\omega) - V_1^* G_{\mathbf{k}1\sigma, 1\sigma}^<(\omega)] \end{aligned} \quad (6)$$

where the Keldysh less Green functions are defined as

$$\begin{aligned} G_{1\sigma, \mathbf{k}1\sigma}^<(t, t') & \equiv i \langle c_{\mathbf{k}1\sigma}^\dagger(t') d_{1\sigma}(t) \rangle, \\ G_{\mathbf{k}1\sigma, 1\sigma}^<(t, t') & \equiv i \langle d_{1\sigma}^\dagger(t') c_{\mathbf{k}1\sigma}(t) \rangle. \end{aligned} \quad (7)$$

By using the Keldysh Green function formalism, one can obtain the Dyson equations as

$$\begin{aligned} G_{\mathbf{k}1\sigma, 1\sigma}^<(\omega) & = V_1 [g_{\mathbf{k}1\sigma}^t(\omega) G_{1\sigma, 1\sigma}^<(\omega) \\ & \quad - g_{\mathbf{k}1\sigma}^<(\omega) G_{1\sigma, 1\sigma}^t(\omega)], \\ G_{1\sigma, \mathbf{k}1\sigma}^<(\omega) & = V_1^* [g_{\mathbf{k}1\sigma}^<(\omega) G_{1\sigma, 1\sigma}^t(\omega) \\ & \quad - g_{\mathbf{k}1\sigma}^t(\omega) G_{1\sigma, 1\sigma}^<(\omega)], \end{aligned} \quad (8)$$

where the Keldysh less Green function for electrons in dot 1 is defined as

$$G_{1\sigma, 1\sigma}^<(t, t') \equiv i \langle d_{1\sigma}^\dagger(t') d_{1\sigma}(t) \rangle, \quad (9)$$

and $g_{\mathbf{k}1\sigma}$ is the Green functions for noninteracting electrons of the lead 1. The time-ordered and anti-time-ordered Green functions are denoted by the superscripts t and \bar{t} , respectively. Therefore, the current from the lead 1 (or 2) to the dot 1 can be expressed as

$$J_{1(2)} = \frac{ie}{\hbar} \sum_{\sigma} \int \frac{d\epsilon}{2\pi} \Gamma_{1(2)}(\epsilon) \{ G_{1\sigma,1\sigma}^<(\epsilon) + f_{1(2)}(\epsilon) [G_{1\sigma,1\sigma}^r(\epsilon) - G_{1\sigma,1\sigma}^a(\epsilon)] \}, \quad (10)$$

where the line-width $\Gamma_{1(2)} = 2\pi\rho_F V_{1(2)}^2$ with ρ_F the density of states of leads, and $f_{1(2)}(\epsilon)$ is the Fermi-Dirac distribution functions of the lead 1 (or 2) with the chemical potential $\mu_{1(2)}$. Here we have assumed that the leads give rise to a flat, energy independent, density of states (i. e., the wide-band limit). By applying the similar procedure, the currents from the leads 3 and 4 to the dot 2 are found similarly,

$$J_{3(4)} = \frac{ie}{\hbar} \sum_{\sigma} \int \frac{d\epsilon}{2\pi} \Gamma_{3(4)}(\epsilon) \{ G_{2\sigma,2\sigma}^<(\epsilon) + f_{3(4)}(\epsilon) [G_{2\sigma,2\sigma}^r(\epsilon) - G_{2\sigma,2\sigma}^a(\epsilon)] \}, \quad (11)$$

with $\Gamma_{3(4)} = 2\pi\rho_F V_{3(4)}^2$ for the lead 3 (or 4).

Under the symmetric condition: $\mu_1 + \mu_2 = \mu_3 + \mu_4$, there is no current between dot 1 and dot 2. In the steady state, the current will be uniform, so that the current through dot 1 satisfies $J_{dot1} = J_1 = -J_2$, and then one can symmetrize the current through the dot 1 as

$$\begin{aligned} J_{dot1} &= \frac{1}{2} (J_1 - J_2) \\ &= i \frac{e}{2\hbar} \sum_{\sigma} \int \frac{d\epsilon}{2\pi} [(f_1 \Gamma_1 - f_2 \Gamma_2) (G_{1\sigma,1\sigma}^r(\epsilon) - G_{1\sigma,1\sigma}^a(\epsilon)) + (\Gamma_1 - \Gamma_2) G_{1\sigma,1\sigma}^<(\epsilon)], \end{aligned} \quad (12)$$

and similarly the current through the dot 2 is

$$\begin{aligned} J_{dot2} &= i \frac{e}{2\hbar} \sum_{\sigma} \int \frac{d\epsilon}{2\pi} [(f_3 \Gamma_3 - f_4 \Gamma_4) (G_{2\sigma,2\sigma}^r(\epsilon) - G_{2\sigma,2\sigma}^a(\epsilon)) + (\Gamma_3 - \Gamma_4) G_{2\sigma,2\sigma}^<(\epsilon)]. \end{aligned} \quad (13)$$

It is noted that Eqs. (12) and (13) give rise to the current through each dot of the DQD system in terms of the distribution functions of leads and the local properties of dots. In order to obtain the current, one has to compute the retarded and the Keldysh less Green functions of the DQD system in the presence of both the interdot tunneling coupling t and intradot Coulomb interaction U as well as the tunneling coupling of DQD system into the leads.

Without the loss of generality, we assume that the dot-lead tunneling coupling are symmetric: $\Gamma_1 = \Gamma_2 = \Gamma_3 = \Gamma_4 = \Gamma$, and the symmetric configuration of the chemical potentials: $\mu_1 = \mu_3 = \mu + eV/2$, and $\mu_2 = \mu_4 = \mu - eV/2$.

Then the current through the dot 1 (or 2) becomes

$$J_{dot1(2)} = \frac{e\Gamma}{2\hbar} \sum_{\sigma} \int d\epsilon [f_1(\epsilon) - f_2(\epsilon)] \mathcal{A}_{1(2)\sigma}(\epsilon), \quad (14)$$

where the dot spectral functions are defined as

$$\mathcal{A}_{1(2)\sigma} = (-1/\pi) \text{Im} [G_{1(2)\sigma,1(2)\sigma}^r]. \quad (15)$$

The associated differential conductance at $\mu = 0$ is found to be

$$\begin{aligned} \frac{dJ_{dot1(2)}}{dV} &= \frac{e^2 \beta \Gamma}{4\hbar} \sum_{\sigma} \int d\epsilon \mathcal{A}_{1(2)\sigma}(\epsilon) \\ &\times \left[\frac{e^{\beta(\epsilon - \frac{eV}{2})}}{\left(e^{\beta(\epsilon - \frac{eV}{2})} + 1 \right)^2} + \frac{e^{\beta(\epsilon + \frac{eV}{2})}}{\left(e^{\beta(\epsilon + \frac{eV}{2})} + 1 \right)^2} \right], \end{aligned} \quad (16)$$

and the linear conductance at zero bias is thus given by

$$G_{dot1(2)} = \frac{e^2 \Gamma}{2\hbar} \sum_{\sigma} \int d\epsilon \left(-\frac{\partial f_{FD}(\epsilon)}{\partial \epsilon} \right) \mathcal{A}_{1(2)\sigma}(\epsilon), \quad (17)$$

where $f_{FD}(\epsilon)$ is the Fermi-Dirac distribution function.

III. THE NONINTERACTING DOTS

In this section we study the case of noninteracting dots, i. e., $U = 0$. In this case, we can exactly derive the Green functions, the associated spectral, and transport properties of the DQD system, which shows the clear evidence of correlated electron transport through DQD.

By applying the equation-of-motion approach, we have

$$\begin{aligned} &(i\omega_n - \epsilon_1) \langle \langle d_{1\sigma} | d_{1\sigma}^{\dagger} \rangle \rangle \\ &= 1 - t \langle \langle d_{2\sigma} | d_{1\sigma}^{\dagger} \rangle \rangle + V_1^* \sum_{\mathbf{k}} \langle \langle c_{\mathbf{k}1\sigma} | d_{1\sigma}^{\dagger} \rangle \rangle \\ &\quad + V_2^* \sum_{\mathbf{k}} \langle \langle c_{\mathbf{k}2\sigma} | d_{1\sigma}^{\dagger} \rangle \rangle, \end{aligned} \quad (18)$$

$$(i\omega_n - \epsilon_{\mathbf{k}1}) \langle \langle c_{\mathbf{k}1\sigma} | d_{1\sigma}^{\dagger} \rangle \rangle = V_1 \langle \langle d_{1\sigma} | d_{1\sigma}^{\dagger} \rangle \rangle, \quad (19)$$

$$(i\omega_n - \epsilon_{\mathbf{k}2}) \langle \langle c_{\mathbf{k}2\sigma} | d_{1\sigma}^{\dagger} \rangle \rangle = V_2 \langle \langle d_{1\sigma} | d_{1\sigma}^{\dagger} \rangle \rangle. \quad (20)$$

Here we assume that the conduction leads have a flat and energy independent density of states (i. e., the wide-band limit), leading to

$$\begin{aligned} -\frac{V_1^2}{N} \sum_{\mathbf{k}} \frac{1}{i\omega_n - \epsilon_{\mathbf{k}1}} &\approx i\pi\rho_F V_1^2 \equiv i\frac{\Gamma_1}{2}, \\ -\frac{V_2^2}{N} \sum_{\mathbf{k}} \frac{1}{i\omega_n - \epsilon_{\mathbf{k}2}} &\approx i\pi\rho_F V_2^2 \equiv i\frac{\Gamma_2}{2}, \end{aligned}$$

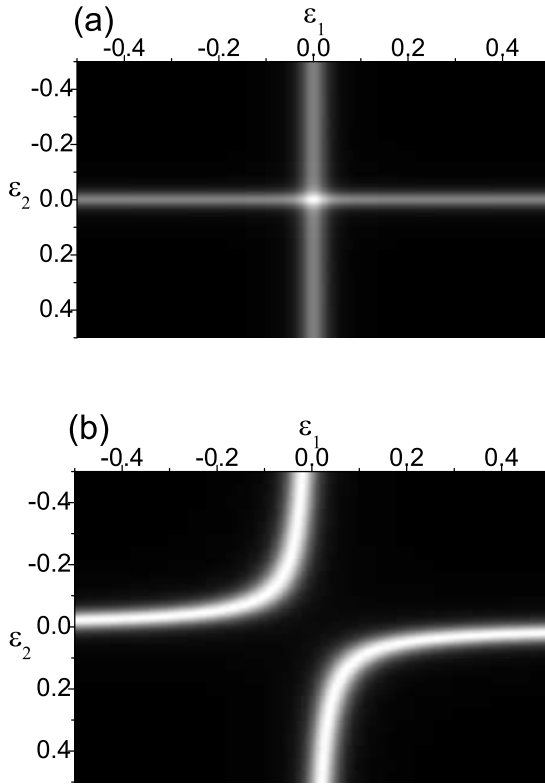


FIG. 2: The images of total linear conductance $G_{dot1} + G_{dot2}$ as a function of the dot levels ϵ_1 and ϵ_2 for noninteracting ($U = 0$) double dots with $\Gamma = 0.01$, $k_B T = 0.01$, $t = 0$ in (a), and $t = 0.1$ in (b).

and then

$$\left[i\omega_n - \epsilon_1 + \frac{i}{2} (\Gamma_1 + \Gamma_2) \right] \langle \langle d_{1\sigma} | d_{1\sigma}^\dagger \rangle \rangle + t \langle \langle d_{2\sigma} | d_{1\sigma}^\dagger \rangle \rangle = 1. \quad (21)$$

By applying the similar method, we obtain the equation of motion for the Green function $\langle \langle d_{2\sigma} | d_{1\sigma}^\dagger \rangle \rangle$ as

$$\left[i\omega_n - \epsilon_2 + \frac{i}{2} (\Gamma_3 + \Gamma_4) \right] \langle \langle d_{2\sigma} | d_{1\sigma}^\dagger \rangle \rangle + t \langle \langle d_{1\sigma} | d_{1\sigma}^\dagger \rangle \rangle = 0. \quad (22)$$

From the above two equations and performing the analytic continuations, we can deduce the retarded Green functions in the symmetric dot-lead tunneling coupling case,

$$G_{1\sigma,1\sigma}^r = \left(\frac{\epsilon_+ - \epsilon_2}{\epsilon_+ - \epsilon_-} \right) \frac{1}{\omega - \epsilon_+ + i\Gamma} + \left(\frac{\epsilon_2 - \epsilon_-}{\epsilon_+ - \epsilon_-} \right) \frac{1}{\omega - \epsilon_- + i\Gamma},$$

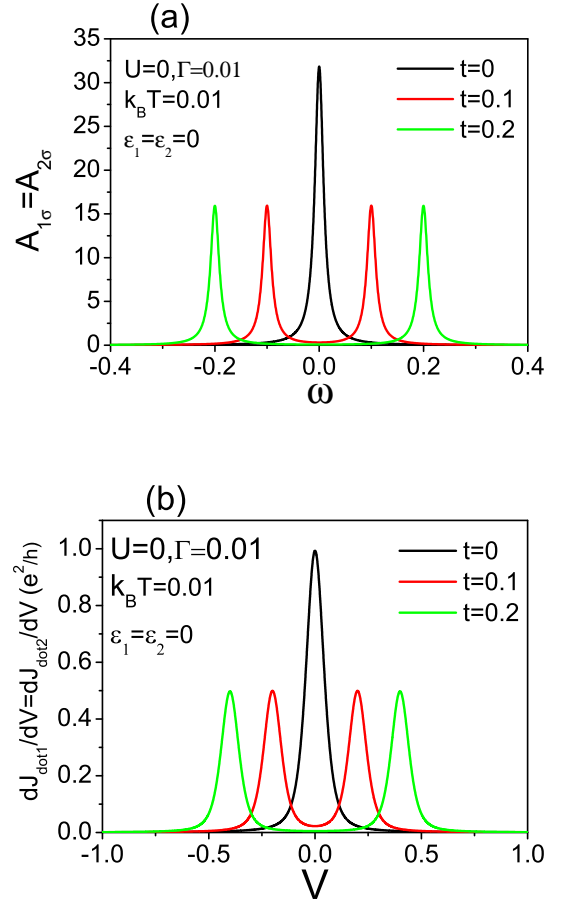


FIG. 3: The spectral function as a function of frequency in (a), and the differential conductance as a function of bias voltage in (b) with the dot-level: $\epsilon_1 = \epsilon_2 = 0$ for different interdot tunneling couplings.

$$G_{2\sigma,2\sigma}^r = \left(\frac{\epsilon_+ - \epsilon_1}{\epsilon_+ - \epsilon_-} \right) \frac{1}{\omega - \epsilon_+ + i\Gamma} + \left(\frac{\epsilon_1 - \epsilon_-}{\epsilon_+ - \epsilon_-} \right) \frac{1}{\omega - \epsilon_- + i\Gamma},$$

and

$$G_{1\sigma,2\sigma}^r = G_{2\sigma,1\sigma}^r = \left(\frac{t}{\epsilon_+ - \epsilon_-} \right) \times \left[\frac{1}{\omega - \epsilon_+ + i\Gamma} - \frac{1}{\omega - \epsilon_- + i\Gamma} \right], \quad (23)$$

where

$$\epsilon_{\pm} = \frac{1}{2} \left[(\epsilon_1 + \epsilon_2) \pm \sqrt{(\epsilon_1 - \epsilon_2)^2 + 4t^2} \right], \quad (24)$$

denote the energies of antibonding and bonding molecular resonant-tunneling states, respectively. Note that the bonding state moves down in energy with the interdot tunneling coupling and the antibonding state moves

up. The energy difference between the antibonding and bonding states is $\epsilon_+ - \epsilon_- = \sqrt{(\epsilon_1 - \epsilon_2)^2 + 4t^2}$. When the levels of two dots cross, i. e. $\epsilon_1 = \epsilon_2$, one has an anticrossing of ϵ_+ and ϵ_- with the minimum antibonding-bonding energy difference $2t$. For large dot-level energy difference, the eigenenergies of tunneling-coupled double dots approach to the energy levels of uncoupled dots, ϵ_1 and ϵ_2 .

From the retarded Green functions, the spectral function of dot 1 is found to be

$$\mathcal{A}_{1\sigma}(\omega) = \frac{1}{\pi} \left[\left(\frac{\epsilon_+ - \epsilon_2}{\epsilon_+ - \epsilon_-} \right) \frac{\Gamma}{(\omega - \epsilon_+)^2 + \Gamma^2} + \left(\frac{\epsilon_2 - \epsilon_-}{\epsilon_+ - \epsilon_-} \right) \frac{\Gamma}{(\omega - \epsilon_-)^2 + \Gamma^2} \right], \quad (25)$$

and changing the index $1 \leftrightarrow 2$ gives the spectral function of dot 2. The spectral functions of dot 1 and 2 display two Lorentzian resonances at the same positions: ϵ_{\pm} , while the ratio of their heights is $(\epsilon_+ - \epsilon_2) / (\epsilon_2 - \epsilon_-)$ for the dot 1, and $(\epsilon_+ - \epsilon_1) / (\epsilon_1 - \epsilon_-)$ for the dot 2.

In Fig. 2 we show the images of the total linear conductance $G_{dot1} + G_{dot2}$, obtained by Eq. (17), versus changes of levels ϵ_1 and ϵ_2 of two dots. The bright regions correspond to high conductance and the dark regions to low conductance. For completely decoupled dots ($t = 0$) as in Fig. 2(a), tuning the level of one dot changes the charge on this dot without affecting the charge on the other dot. For nonzero interdot tunneling coupling, a similar "anticrossing" occurs at $\epsilon_1 = \epsilon_2$ in the diagram of conductance [see Fig. 2(b)].

In Fig. 3, the spectral function and the differential conductance of dots are displayed for $\epsilon_1 = \epsilon_2 = 0$ and different interdot tunneling couplings. In the absence of interdot tunneling, the electron transports through each dot independently, which exhibits a resonant peak when the dot levels match the chemical potential of the leads. Increasing the interdot tunneling leads to the splitting of resonant peak at the positions ϵ_{\pm} , corresponding to the bonding and antibonding molecular states of the DQD system. Tuning the bias voltage gives rise to the resonances in the differential conductance when the resonant peaks in the spectral function enter the region between the chemical potentials of leads.

We also show the spectral function and the differential conductance of dots along the direction $\epsilon_1 = \epsilon_2$ for different interdot tunneling couplings in Fig. 4. Compared to Fig. 3, the spectral function is shifted to $\epsilon_1 = \epsilon_2 = 0.1$. The asymmetric spectral function along ω leads to the four peaks structure in the differential conductance as a function of the bias voltage for the general configuration of dot level and the finite interdot tunneling coupling [see the green line of Fig. 4(b)]. One interesting observation is that under the condition $t = \epsilon_1 = \epsilon_2$, this general four peaks structure reduces to the three peaks structure [see the red line of Fig. 4(b)], while in this case the antibonding energy shifts to zero [see the red line of correspond-

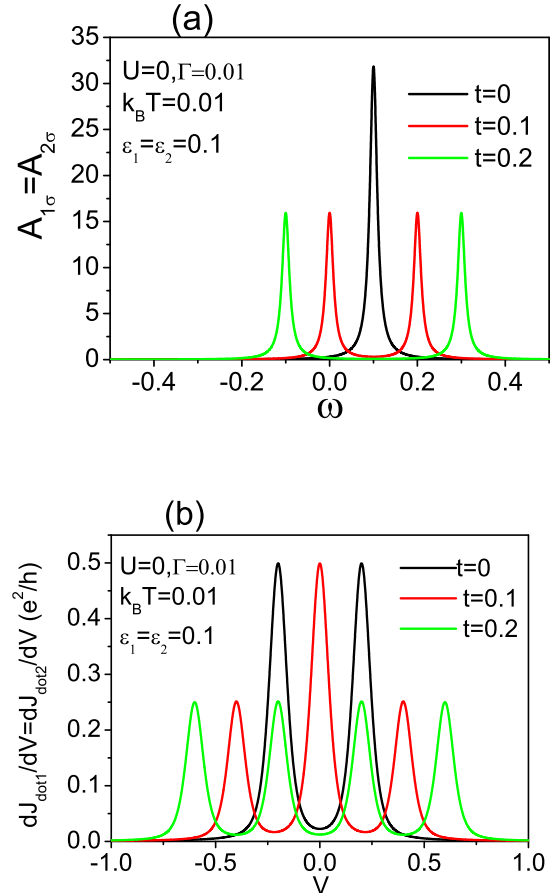


FIG. 4: The spectral function (a) and the differential conductance (b) with the dot-level: $\epsilon_1 = \epsilon_2 = 0.1$ for different interdot tunneling coupling.

ing spectral function in Fig. 4(a)]. This feature offers a possible method to measure the tunneling coupling between dots in experiments. Fig. 5 displays the spectral function and the differential conductance along the direction $\epsilon_1 = -\epsilon_2 = -\epsilon_d$ for different interdot tunneling couplings. In this case, from Eq. (24) one can easily see that the bonding and antibonding energies reduce to $\epsilon_{\pm} = \pm(\epsilon_d + t)$, which yields two resonant peaks in the spectral function for finite interdot tunneling coupling, while the heights of these two peaks are different for the ratio of heights is $t/(2\epsilon_d + t)$ for dot 1 and $(2\epsilon_d + t)/t$ for dot 2. As these two resonant peaks sit at the positions with the same absolute value, there are only two resonances in the differential conductance compared to the four resonances in the case $\epsilon_1 = \epsilon_2$ (see Fig. 5).

In Fig. 6, the linear conductance of each dot as a function of one dot's level is displayed by setting another dot's level. In the absence of the interdot tunneling coupling, electron transports independently through each dot, which shows one constant linear conductance of dot 1 and one resonant peak in the linear conductance of dot

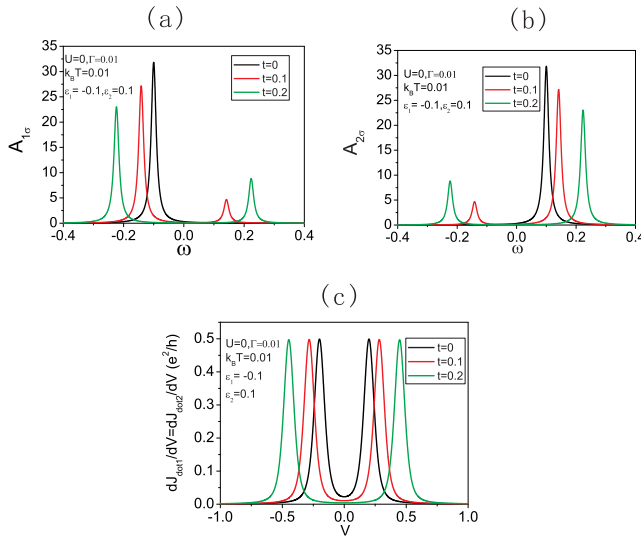


FIG. 5: The spectral function of the dot 1 in (a) and the dot 2 in (b) and the differential conductance in (c) with the dot-level: $\epsilon_1 = -0.1, \epsilon_2 = 0.1$ for different interdot tunneling coupling.

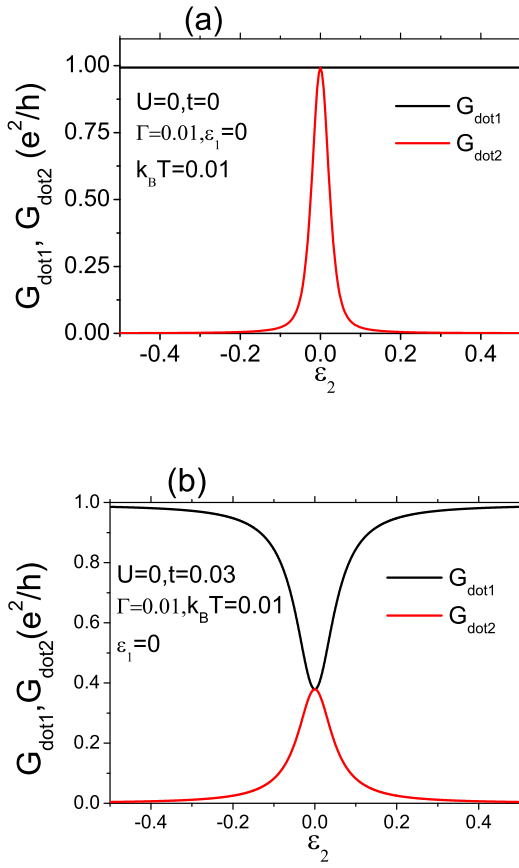


FIG. 6: The linear conductance of dot 1 and 2 as a function of dot level of one dot ϵ_2 by setting another dot's level as $\epsilon_1 = 0$ without (a) and with (b) the interdot tunneling coupling.

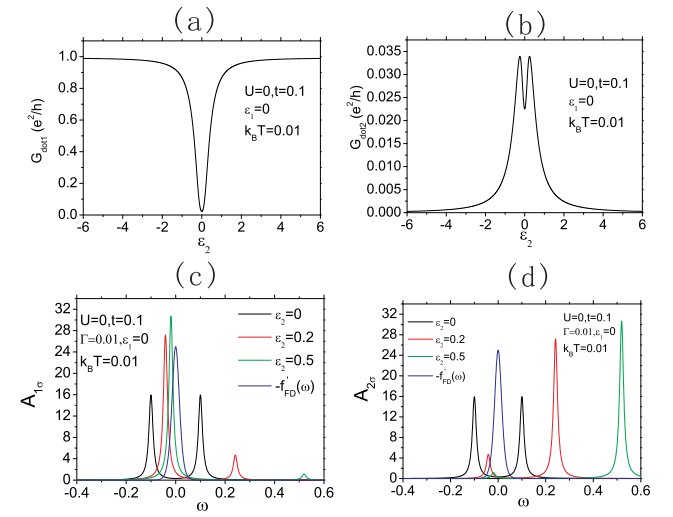


FIG. 7: The linear conductance of dot 1 (a) and 2 (b) as a function of dot level of one dot ϵ_2 by setting another dot's level as $\epsilon_1 = 0$ when increasing the interdot tunneling coupling, and the associated spectral functions for different ϵ_2 [(c) and (d)].

2 when ϵ_2 matches the chemical potential of leads. In the presence of interdot tunneling coupling, the linear conductance of dot 1 shows a dip at the same position of ϵ_2 , where the linear conductance of dot 2 exhibits a resonant peak.

An interesting feature is shown in Fig. 7 when increasing the interdot tunneling coupling: the resonant peak in the linear conductance of dot 2 is suppressed into two splitting peaks. Both the dip in G_{dot1} and the splitting peaks in G_{dot2} could be understood with the help of the associated spectral function of each dot for different dot level ϵ_2 . The blue line in $A_{1(2)\sigma}$ of Fig. 7 shows $-\partial f_{FD}/\partial \epsilon$ in the formula of linear conductance Eq. (17), which sets the window of temperature. It is noted that the spectral functions of both dots will include two peaks, corresponding to the bonding and antibonding states at finite interdot tunneling coupling, while the heights of these two peaks are different. For the spectral function of dot 1 ($A_{1\sigma}$), when increasing the dot level ϵ_2 , the peak corresponding to bonding state ϵ_- , which is smaller than the minimum of ϵ_1 and ϵ_2 , moves to the window of temperature with the increasing of its height. This will enhance the linear conductance of dot 1 as increasing ϵ_2 from $\epsilon_2 = 0$, and the linear conductance saturates to a constant value as the bonding-state peak completely enter into the window of temperature [see Fig. 7(a)]. For the spectral function of dot 2 ($A_{2\sigma}$), as increasing the dot level ϵ_2 , the bonding-state peak moves into the window of temperature, but the height of this peak decreases. This leads to a maximum in linear conductance of dot 2 [see Fig. 7(b)]. While this maximum in the linear conductance of dot 2 could not be observed in the small interdot coupling case (as shown in Fig. 6) or in the low temperature case, because the bonding-state peak is

too close to $\omega = 0$ or the window of temperature is too narrow.

IV. THE INTERACTING DOTS

In this section we study the transport phenomena through tunneling-coupled DQD system with intradot Coulomb interaction with the help of equation-of-motion approach. This method consists of differentiating the Green function with respect to time, thereby generating higher-order Green functions in the presence of intradot on-site Coulomb interaction which eventually have to be

closed. Here we apply the Hartree-Fock approximation to truncate the higher-order Green functions, which includes the contributions of higher order electron tunneling processes. It is known that the Hartree-Fock approximation captures the correct qualitative feature of physics of single quantum dot in the Coulomb blockade regime, valid in the higher temperature regime.

By applying the equation-of-motion approach and the Hartree-Fock approximation to truncate the higher-order Green functions (for detailed calculation see the Appendix A), we obtain the Green functions for dot electrons as

$$\langle\langle d_{1\sigma} | d_{1\sigma}^\dagger \rangle\rangle = \frac{F_1 [i\omega_n - \epsilon_2 + F_2 \frac{i}{2} (\Gamma_3 + \Gamma_4)]}{[i\omega_n - \epsilon_1 + F_1 \frac{i(\Gamma_1 + \Gamma_2)}{2}] [i\omega_n - \epsilon_2 + F_2 \frac{i(\Gamma_3 + \Gamma_4)}{2}] - t^2 F_1 F_2}, \quad (26)$$

$$\langle\langle d_{2\sigma} | d_{2\sigma}^\dagger \rangle\rangle = \frac{F_2 [i\omega_n - \epsilon_1 + F_1 \frac{i}{2} (\Gamma_1 + \Gamma_2)]}{[i\omega_n - \epsilon_1 + F_1 \frac{i(\Gamma_1 + \Gamma_2)}{2}] [i\omega_n - \epsilon_2 + F_2 \frac{i(\Gamma_3 + \Gamma_4)}{2}] - t^2 F_1 F_2}, \quad (27)$$

and

$$\langle\langle d_{2\sigma} | d_{1\sigma}^\dagger \rangle\rangle = \langle\langle d_{1\sigma} | d_{2\sigma}^\dagger \rangle\rangle \frac{-t F_1 F_2}{[i\omega_n - \epsilon_1 + F_1 \frac{i(\Gamma_1 + \Gamma_2)}{2}] [i\omega_n - \epsilon_2 + F_2 \frac{i(\Gamma_3 + \Gamma_4)}{2}] - t^2 F_1 F_2}, \quad (28)$$

where

$$\begin{aligned} F_1(i\omega_n, \epsilon_1, \langle n_{1\bar{\sigma}} \rangle) &= 1 + \frac{U \langle n_{1\bar{\sigma}} \rangle}{i\omega_n - \epsilon_1 - U}, \\ F_2(i\omega_n, \epsilon_2, \langle n_{2\bar{\sigma}} \rangle) &= 1 + \frac{U \langle n_{2\bar{\sigma}} \rangle}{i\omega_n - \epsilon_2 - U}. \end{aligned} \quad (29)$$

Performing the analytic continuations, we can deduce the retarded Green functions for dot electrons in the tunneling-coupled DQD system with intradot on-site Coulomb interaction: $G_{i\sigma, j\sigma}^r$, where $i, j = 1, 2$ corresponding dot 1 and 2 respectively. The occupation numbers are subjected to the self-consistency condition:

$$\langle n_{i\sigma} \rangle = -i \int \frac{d\omega}{2\pi} G_{i\sigma, i\sigma}^<(\omega), \quad (30)$$

where $i = 1$ and 2.

Next we calculate the Keldysh less Green functions $G_{i\sigma, i\sigma}^<(\omega)$, which is needed in the self-consistent equation Eq. (30) for the dot occupation numbers. Under the same Hartree-Fock approximation as in the retarded Green functions, the equation of motion approach gives that the Keldysh less Green functions satisfy (for detailed calculation see the Appendix B)

$$\begin{aligned} G_{1\sigma, 1\sigma}^< &= i [\Gamma_1 f_1(\omega) + \Gamma_2 f_2(\omega)] G_{1\sigma, 1\sigma}^r G_{1\sigma, 1\sigma}^a \\ &+ i [\Gamma_3 f_3(\omega) + \Gamma_4 f_4(\omega)] G_{2\sigma, 1\sigma}^r G_{2\sigma, 1\sigma}^a, \end{aligned} \quad (31)$$

for dot 1, and

$$\begin{aligned} G_{2\sigma, 2\sigma}^< &= i [\Gamma_1 f_1(\omega) + \Gamma_2 f_2(\omega)] G_{1\sigma, 2\sigma}^r G_{1\sigma, 2\sigma}^a \\ &+ i [\Gamma_3 f_3(\omega) + \Gamma_4 f_4(\omega)] G_{2\sigma, 2\sigma}^r G_{2\sigma, 2\sigma}^a, \end{aligned} \quad (32)$$

for dot 2.

Fig. 8 shows the images of the total linear conductance $G_{dot1} + G_{dot2}$ of DQD with the intradot on-site Coulomb interaction versus the changes of the dot-level ϵ_1 and ϵ_2 . Without interdot tunneling coupling, the images of conductance shows a square lattice structure [see Fig. 8(a)]. In the presence of both the interdot tunneling coupling and the intradot Coulomb interaction, the "anticrossing" occurs at the positions of ϵ_1 , ϵ_2 , $\epsilon_1 + U$, and $\epsilon_2 + U$ [see Fig. 8(b)].

The effects of the intradot Coulomb interaction and the interdot tunneling coupling can be clearly shown in the spectral functions of quantum dots. Fig. 9 is the spectral function and the differential conductance of the dot 1. In the absence of the interdot tunneling coupling, the intradot Coulomb interaction leads to two peaks at $\epsilon_{1(2)}$ and $\epsilon_{1(2)} + U$ in the spectral function, in agreement with the well-known result of Coulomb blockade at higher temperatures. These two peaks split in the presence of the interdot tunneling coupling, and the spectral function displays a four peak structure. The differential

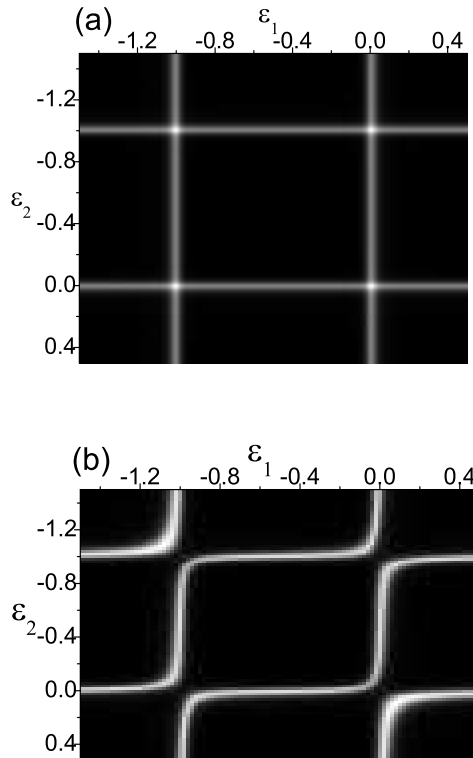


FIG. 8: The images of total linear conductance $G_{dot1} + G_{dot2}$ as a function of the dot levels ϵ_1 and ϵ_2 for interacting ($U = 1$) double dots with $\Gamma = 0.01$, $k_B T = 0.01$ $t = 0$ in (a), and $t = 0.1$ in (b).

conductance exhibits the resonance peaks when the spectral function peaks enter the window of bias voltage. Due to the small size of QD, the Coulomb charging energy U becomes the largest energy scale. In the case $U > t$, the peaks in both the spectral function and the linear conductance form two distinct groups separated by roughly the intradot Coulomb interaction U , while in each group there are two peaks separated by roughly the interdot tunneling coupling t .

In Fig. 10 we show the linear conductance of each dot with the intradot Coulomb interaction as a function of one dot-level by setting another dot-level. In the absence of interdot tunneling coupling, by setting ϵ_1 and tuning ϵ_2 , G_{dot1} remains constant and G_{dot2} shows two resonant peaks when the levels ϵ_2 and $\epsilon_2 + U$ match the chemical potential of leads. Due to the interdot tunneling coupling, the electron transport through one dot is strongly influenced by the electron transport through another dot: G_{dot1} displays two dips at the corresponding resonant positions of G_{dot2} . This feature provides a possible experimental method to observe the correlated electron transport phenomena in the real interacting DQD system with strong intradot tunneling coupling at high temperatures.

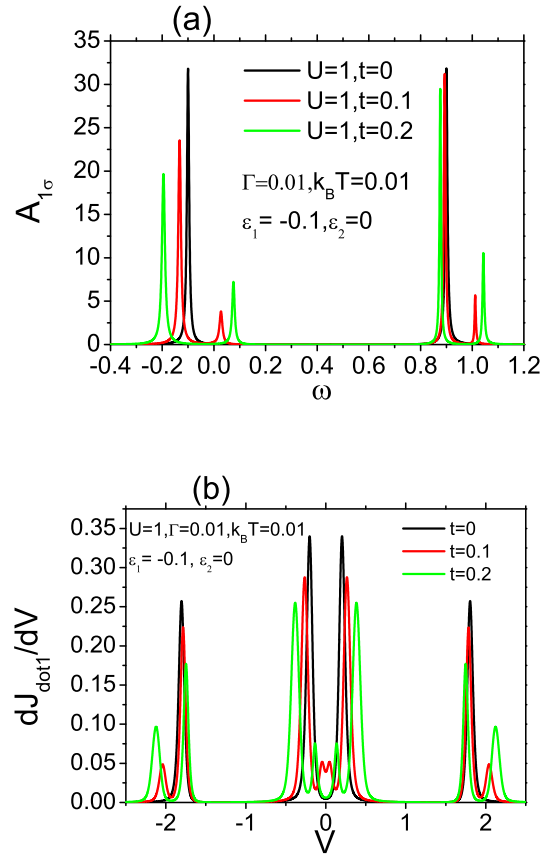


FIG. 9: The spectral function (a) and the differential conductance (b) of the dot 1 in the DQD system with the intradot Coulomb interaction in the general case of the dot-level: $\epsilon_1 = -0.1$, $\epsilon_2 = 0$ for different interdot tunneling coupling.

V. SUMMARY

In this work we have investigated theoretically the electron transport through parallel tunneling-coupled DQD system with the special configuration that two leads are connected to each dot. By applying the Keldysh nonequilibrium Green function technique and the equation-of-motion approach, we have obtained the spectral and conductance spectra of DQD with and without the intradot on-site Coulomb interaction, respectively.

The main results are summarized as following:

1) In the absence of intradot Coulomb interaction, the exact results of the spectral function and the conductance are obtained, showing resonant peaks at the positions of antibonding and bonding molecular states for finite interdot tunneling couplings, while the heights of these resonant peaks depend on the levels of two dots.

2) Tuning the dot levels results in different structure of the differential conductance, e. g., under the condition $\epsilon_1 = \epsilon_2 = t$, the general four-peak structure in the dif-

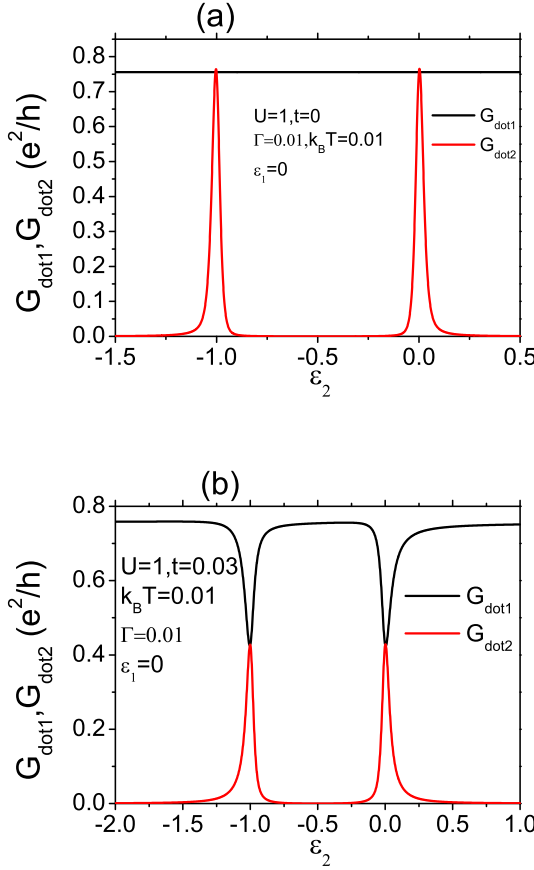


FIG. 10: The linear conductance of dot 1 and 2 with the intradot-dot Coulomb interaction as a function of dot level of one dot ϵ_2 by setting another dot's level as $\epsilon_1 = 0$ without [in (a)] and with [in (b)] the interdot tunneling coupling.

ferential conductance can reduce to the three-peak structure.

3) For DQD with the intradot Coulomb interaction, the Hartree-Fock approximation has been applied to calculate both the retarded and the Keldysh less Green functions, which gives the transport properties at high temperatures.

4) As the interdot Coulomb interaction U becomes the largest energy scale of quantum dot in the single-electron tunneling regime, the peaks in the spectral function and the conductance form two groups separated by roughly U , and the interdot tunneling coupling t induces the splitting of peaks in each group.

5) The linear conductance of each dot shows the phenomena of correlated electron transport through tunneling-coupled DQD system, which could be observed with the present experimental techniques.

Acknowledgments

R. Lü is supported by the MOE of China (Grant No.200221). G.M. Zhang is supported by NSF-China (Grant No.10125418) and the Special Fund for Major State Basic Research Projects of China (Grant No.G2000067107).

APPENDIX A: THE EVALUATION OF RETARDED GREEN FUNCTIONS

In this Appendix, we give the detailed evaluation of the retarded Green functions for dot electrons in the tunneling-coupled DQD with intradot on-site Coulomb interaction based on the equation-of-motion approach. Its equation of motion is yielded as

$$(i\omega_n - \epsilon_1) \langle \langle d_{1\sigma} | d_{1\sigma}^\dagger \rangle \rangle = 1 - t \langle \langle d_{2\sigma} | d_{1\sigma}^\dagger \rangle \rangle + U \langle \langle n_{1\bar{\sigma}} d_{1\sigma} | d_{1\sigma}^\dagger \rangle \rangle + V_1^* \sum_{\mathbf{k}} \langle \langle c_{\mathbf{k}1\sigma} | d_{1\sigma}^\dagger \rangle \rangle + V_2^* \sum_{\mathbf{k}} \langle \langle c_{\mathbf{k}2\sigma} | d_{1\sigma}^\dagger \rangle \rangle \quad (A1)$$

$$(i\omega_n - \epsilon_{\mathbf{k}1}) \langle \langle c_{\mathbf{k}1\sigma} | d_{1\sigma}^\dagger \rangle \rangle = V_1 \langle \langle d_{1\sigma} | d_{1\sigma}^\dagger \rangle \rangle, \quad (A2)$$

$$(i\omega_n - \epsilon_{\mathbf{k}2}) \langle \langle c_{\mathbf{k}2\sigma} | d_{1\sigma}^\dagger \rangle \rangle = V_2 \langle \langle d_{1\sigma} | d_{1\sigma}^\dagger \rangle \rangle, \quad (A3)$$

where the higher-order Green function $\langle \langle n_{1\bar{\sigma}} d_{1\sigma} | d_{1\sigma}^\dagger \rangle \rangle$ is generated. The equation of motion of $\langle \langle n_{1\bar{\sigma}} d_{1\sigma} | d_{1\sigma}^\dagger \rangle \rangle$ can be further deduced to

$$\begin{aligned} & (i\omega_n - \epsilon_1 - U) \langle \langle n_{1\bar{\sigma}} d_{1\sigma} | d_{1\sigma}^\dagger \rangle \rangle \\ &= \langle n_{1\bar{\sigma}} \rangle - t \left(\langle \langle n_{1\bar{\sigma}} d_{2\sigma} | d_{1\sigma}^\dagger \rangle \rangle + \langle \langle d_{1\bar{\sigma}}^\dagger d_{2\bar{\sigma}} d_{1\sigma} | d_{1\sigma}^\dagger \rangle \rangle \right. \\ & \quad \left. - \langle \langle d_{2\bar{\sigma}}^\dagger d_{1\bar{\sigma}} d_{1\sigma} | d_{1\sigma}^\dagger \rangle \rangle \right) \\ & \quad - \sum_{\mathbf{k}} \left(V_1 \langle \langle c_{\mathbf{k}1\bar{\sigma}}^\dagger d_{1\bar{\sigma}} d_{1\sigma} | d_{1\sigma}^\dagger \rangle \rangle - V_1^* \langle \langle n_{1\bar{\sigma}} c_{\mathbf{k}1\sigma} | d_{1\sigma}^\dagger \rangle \rangle \right. \\ & \quad \left. - V_1^* \langle \langle d_{1\bar{\sigma}}^\dagger c_{\mathbf{k}1\bar{\sigma}} d_{1\sigma} | d_{1\sigma}^\dagger \rangle \rangle \right). \end{aligned} \quad (A4)$$

Making the Hartree-Fock approximation to decouple the higher-order Green functions in the above equation:

$$\begin{aligned} \langle \langle d_{1\bar{\sigma}}^\dagger d_{2\bar{\sigma}} d_{1\sigma} | d_{1\sigma}^\dagger \rangle \rangle &\simeq \langle d_{1\bar{\sigma}}^\dagger d_{2\bar{\sigma}} \rangle \langle \langle d_{1\sigma} | d_{1\sigma}^\dagger \rangle \rangle, \\ \langle \langle d_{2\bar{\sigma}}^\dagger d_{1\bar{\sigma}} d_{1\sigma} | d_{1\sigma}^\dagger \rangle \rangle &\simeq \langle d_{2\bar{\sigma}}^\dagger d_{1\bar{\sigma}} \rangle \langle \langle d_{1\sigma} | d_{1\sigma}^\dagger \rangle \rangle, \\ \langle \langle c_{\mathbf{k}1\bar{\sigma}}^\dagger d_{1\bar{\sigma}} d_{1\sigma} | d_{1\sigma}^\dagger \rangle \rangle &\simeq \langle c_{\mathbf{k}1\bar{\sigma}}^\dagger d_{1\bar{\sigma}} \rangle \langle \langle d_{1\sigma} | d_{1\sigma}^\dagger \rangle \rangle, \\ \langle \langle d_{1\bar{\sigma}}^\dagger c_{\mathbf{k}1\bar{\sigma}} d_{1\sigma} | d_{1\sigma}^\dagger \rangle \rangle &\simeq \langle d_{1\bar{\sigma}}^\dagger c_{\mathbf{k}1\bar{\sigma}} \rangle \langle \langle d_{1\sigma} | d_{1\sigma}^\dagger \rangle \rangle. \end{aligned} \quad (A5)$$

and considering the facts: $V_1 = V_1^*$, $\langle d_{1\bar{\sigma}}^\dagger d_{2\bar{\sigma}} \rangle = \langle d_{2\bar{\sigma}}^\dagger d_{1\bar{\sigma}} \rangle$, and $\langle c_{\mathbf{k}1\bar{\sigma}}^\dagger d_{1\bar{\sigma}} \rangle = \langle d_{1\bar{\sigma}}^\dagger c_{\mathbf{k}1\bar{\sigma}} \rangle$, the higher-order Green function is thus derived as

$$\begin{aligned} & \langle \langle n_{1\bar{\sigma}} d_{1\sigma} | d_{1\sigma}^\dagger \rangle \rangle \\ & \simeq \frac{\langle n_{1\bar{\sigma}} \rangle}{i\omega_n - \epsilon_1 - U} \left[1 - t \langle \langle d_{2\sigma} | d_{1\sigma}^\dagger \rangle \rangle \right. \\ & \quad \left. + \left(\sum_{\mathbf{k}} \frac{|V_1|^2}{i\omega_n - \epsilon_{\mathbf{k}1}} + \sum_{\mathbf{k}} \frac{|V_2|^2}{i\omega_n - \epsilon_{\mathbf{k}2}} \right) \right. \\ & \quad \left. \times \langle \langle d_{1\sigma} | d_{1\sigma}^\dagger \rangle \rangle \right]. \end{aligned} \quad (\text{A6})$$

Introducing

$$\begin{aligned} F_1(i\omega_n, \epsilon_1, \langle n_{1\bar{\sigma}} \rangle) &= 1 + \frac{U \langle n_{1\bar{\sigma}} \rangle}{i\omega_n - \epsilon_1 - U}, \\ F_2(i\omega_n, \epsilon_2, \langle n_{2\bar{\sigma}} \rangle) &= 1 + \frac{U \langle n_{2\bar{\sigma}} \rangle}{i\omega_n - \epsilon_2 - U}, \end{aligned} \quad (\text{A7})$$

the dot Green function $\langle \langle d_{1\sigma} | d_{1\sigma}^\dagger \rangle \rangle$ is found to satisfy the following equation:

$$\begin{aligned} & \left[i\omega_n - \epsilon_1 - F_1 \left(\sum_{\mathbf{k}} \frac{|V_1|^2}{i\omega_n - \epsilon_{\mathbf{k}1}} + \sum_{\mathbf{k}} \frac{|V_2|^2}{i\omega_n - \epsilon_{\mathbf{k}2}} \right) \right. \\ & \quad \left. \times \langle \langle d_{1\sigma} | d_{1\sigma}^\dagger \rangle \rangle + t F_1 \langle \langle d_{2\sigma} | d_{1\sigma}^\dagger \rangle \rangle \right] = F_1. \end{aligned} \quad (\text{A8})$$

By applying the similar method, the equation of motion of the Green function $\langle \langle d_{2\sigma} | d_{1\sigma}^\dagger \rangle \rangle$ satisfies:

$$\begin{aligned} & t F_2 \langle \langle d_{1\sigma} | d_{1\sigma}^\dagger \rangle \rangle \\ & + \left[i\omega_n - \epsilon_2 - F_2 \left(\sum_{\mathbf{k}} \frac{|V_3|^2}{i\omega_n - \epsilon_{\mathbf{k}3}} + \sum_{\mathbf{k}} \frac{|V_4|^2}{i\omega_n - \epsilon_{\mathbf{k}4}} \right) \right] \\ & \times \langle \langle d_{2\sigma} | d_{1\sigma}^\dagger \rangle \rangle = 0. \end{aligned} \quad (\text{A9})$$

From the above two equations, we obtain the retarded Green functions as shown in Eqs. (26) and (28). Similarly, we can obtain the retarded Green functions $\langle \langle d_{2\sigma} | d_{2\sigma}^\dagger \rangle \rangle$ and $\langle \langle d_{1\sigma} | d_{2\sigma}^\dagger \rangle \rangle$ as shown in Eqs. (27) and (28).

APPENDIX B: THE EVALUATION OF THE KELDYSH LESS GREEN FUNCTIONS

With the help of equation-of-motion approach, one can also obtain the Keldysh less Green functions, which is

needed in the self-consistent evaluation of the dot occupation numbers when a finite bias voltage is applied across the system. Its equation of motion is yielded as

$$\begin{aligned} & i \frac{\partial}{\partial t} G_{1\sigma,1\sigma}^<(t, t') \\ & = \epsilon_1 i \langle d_{1\sigma}^\dagger(t') d_{1\sigma}(t) \rangle - t i \langle d_{1\sigma}^\dagger(t') d_{2\sigma}(t) \rangle \\ & + U i \langle d_{1\sigma}^\dagger(t') [n_{1\bar{\sigma}} d_{1\sigma}] (t) \rangle + V_1^* \sum_{\mathbf{k}} i \langle d_{1\sigma}^\dagger(t') c_{\mathbf{k}1\sigma}(t) \rangle \\ & + V_2^* \sum_{\mathbf{k}} i \langle d_{1\sigma}^\dagger(t') c_{\mathbf{k}2\sigma}(t) \rangle, \end{aligned} \quad (\text{B1})$$

and then we perform the Fourier transform

$$\begin{aligned} & \omega G_{1\sigma,1\sigma}^<(\omega) \\ & = \epsilon_1 G_{1\sigma,1\sigma}^<(\omega) - t G_{2\sigma,1\sigma}^<(\omega) + V_2^* \sum_{\mathbf{k}} G_{\mathbf{k}2\sigma,1\sigma}^<(\omega) \\ & + U \langle \langle n_{1\bar{\sigma}} d_{1\sigma} | d_{1\sigma}^\dagger \rangle \rangle^<(\omega) + V_1^* \sum_{\mathbf{k}} G_{\mathbf{k}1\sigma,1\sigma}^<(\omega) \end{aligned} \quad (\text{B2})$$

Under the same Hartree-Fock approximation as in the retarded Green functions, the equation of motion for the higher-order Keldysh Green function $\langle \langle n_{1\bar{\sigma}} d_{1\sigma} | d_{1\sigma}^\dagger \rangle \rangle^<$ can also be deduced to

$$\begin{aligned} & (\omega - \epsilon_1 - U) \langle \langle n_{1\bar{\sigma}} d_{1\sigma} | d_{1\sigma}^\dagger \rangle \rangle^<(\omega) \\ & = -t \langle n_{1\bar{\sigma}} \rangle G_{2\sigma,1\sigma}^<(\omega) + V_1^* \langle n_{1\bar{\sigma}} \rangle \sum_{\mathbf{k}} G_{\mathbf{k}1\sigma,1\sigma}^<(\omega) \\ & + V_2^* \langle n_{1\bar{\sigma}} \rangle \sum_{\mathbf{k}} G_{\mathbf{k}2\sigma,1\sigma}^<(\omega). \end{aligned} \quad (\text{B3})$$

By using the exact Dyson equation for $G_{\mathbf{k}1(2)\sigma,1\sigma}^<(\omega)$:

$$\begin{aligned} G_{\mathbf{k}1(2)\sigma,1\sigma}^<(\omega) &= V_1 \left[g_{\mathbf{k}1(2)\sigma}^r(\omega) G_{1\sigma,1\sigma}^<(\omega) \right. \\ & \quad \left. + g_{\mathbf{k}1(2)\sigma}^<(\omega) G_{1\sigma,1\sigma}^a(\omega) \right], \end{aligned} \quad (\text{B4})$$

the equation of motion for the $G_{1\sigma,1\sigma}^<$ becomes

$$\left[\omega - \epsilon_1 - F_1 \left(|V_1|^2 \sum_{\mathbf{k}} g_{\mathbf{k}1\sigma}^r + |V_2|^2 \sum_{\mathbf{k}} g_{\mathbf{k}2\sigma}^r \right) \right] G_{1\sigma,1\sigma}^< + t F_1 G_{2\sigma,1\sigma}^< = F_1 \left[|V_1|^2 \sum_{\mathbf{k}} g_{\mathbf{k}1\sigma}^< + |V_2|^2 \sum_{\mathbf{k}} g_{\mathbf{k}2\sigma}^< \right] G_{1\sigma,1\sigma}^a. \quad (B5)$$

By applying the same method, we obtain the equation of motion for the Keldysh less Green function $G_{2\sigma,1\sigma}^<$ as

$$t F_2 G_{1\sigma,1\sigma}^< + \left[\omega - \epsilon_2 - F_2 \left(|V_3|^2 \sum_{\mathbf{k}} g_{\mathbf{k}3\sigma}^r + |V_4|^2 \sum_{\mathbf{k}} g_{\mathbf{k}4\sigma}^r \right) \right] G_{2\sigma,1\sigma}^< = F_2 \left[|V_3|^2 \sum_{\mathbf{k}} g_{\mathbf{k}3\sigma}^< + |V_4|^2 \sum_{\mathbf{k}} g_{\mathbf{k}4\sigma}^< \right] G_{2\sigma,1\sigma}^a. \quad (B6)$$

From these two equations, we can solve the Keldysh less Green functions as Eq. (31) for dot 1 and Eq. (32) for

dot 2.

¹ For a review, see W. G. van der Wiel, S. De Franceschi, J. M. Elzerman, T. Fujisawa, S. Tarucha, and K. P. Kouwenhoven, Rev. Mod. Phys. **75**, 1 (2003) and references therein.

² For recent experiments, see H. Jeong, A. M. Chang, M. R. Melloch, Science **293**, 2221 (2001); J. C. Chen, A. M. Chang, M. R. Melloch, Phys. Rev. Lett. **92**, 176801 (2004); N. J. Craig, J. M. Taylor, E. A. Lester, C. M. Marcus, M. P. Hanson, A. C. Gossard, Science **304**, 565 (2004).

³ S. A. Wolf, D. D. Awschalom, R. A. Buhrman, J. M. Daughton, S. von Molnár, M. L. Roukes, A. Y. Chtchelkina, and D. M. Treger, Science **294**, 1488 (2001).

⁴ D. D. Awschalom, D. Loss, and N. Samarth, eds., *Semiconductor Spintronics and Quantum Computation* (Springer, Berlin, 2002).

⁵ I. M. Ruzin, V. Chandrasekhar, E. I. Levin, and L. I. Glazman, Phys. Rev. B **45**, 13469 (1992).

⁶ C. Y. Fong, J. S. Nelson, L. A. Hemstreet, R. F. Gallup, L. L. Chang, and L. Esaki, Phys. Rev. B **46**, 9538 (1992).

⁷ J. M. Golden and B. I. Halperin, Phys. Rev. B **53**, 3839 (1996); *ibid*, **54**, 16757 (1996), *ibid*, **56**, 4716 (1997).

⁸ G. Klimeck, G. Chen, and S. Datta, Phys. Rev. B **50**, 2316 (1994); G. Chen, G. Klimeck, S. Datta, G. Chen, and W. A. Goddard III, Phys. Rev. B **50**, 8035 (1994).

⁹ A. A. Middleton and N. S. Wingreen, Phys. Rev. Lett. **71**, 3198 (1993).

¹⁰ C. A. Stafford and S. Das Sarma, Phys. Rev. Lett. **72**, 3590 (1994).

¹¹ K. A. Matveev, L. I. Glazman, and H. U. Baranger, Phys. Rev. B **54**, 5637 (1996).

¹² A. Georges and Y. Mier, Phys. Rev. Lett. **82**, 3805 (1999).

¹³ R. Aguado and D. C. Langreth, Phys. Rev. Lett. **85**, 1946 (2000); Phys. Rev. B **67** 245307 (2003).

¹⁴ T. Aono and M. Eto, Phys. Rev. B **63**, 125327 (2001).

¹⁵ W. Izumida and O. Sakai, Phys. Rev. B **62**, 10260 (2000).

¹⁶ R. López, R. Aguado, and G. Platero, Phys. Rev. Lett. **89**, 136802 (2002).

¹⁷ K. Kikoin and Y. Avishai, Phys. Rev. Lett. **86**, 2090, 2001; Phys. Rev. B **65**, 115329 (2002).

¹⁸ Guang-Ming Zhang, Rong Lü, Zhi-Rong Liu, and Lu Yu, cond-mat/0403629.

¹⁹ T. S. Kim and S. Hershfield, Phys. Rev. B **63**, 245326 (2001).

²⁰ D. Boese, W. Hofstetter, and H. Schoeller, Phys. Rev. B **66**, 125315 (2002).

²¹ P. S. Cornaglia and D. R. Grempel, cond-mat/0408168.

²² U. Wilhelm, J. Schmid, J. Weis, and K. von Klitzing, Physica E **9**, 625 (2001).